Hyperfine fields and field gradients of thin films of face-centred-cubic Fe on Cu(001)

2002 J. Phys.: Condens. Matter 14 12311

(http://iopscience.iop.org/0953-8984/14/47/307)

INSTITUTE OF PHYSICS PUBLISHING JOURNAL OF PHYSICS: CONDENSED MATTER

J. Phys.: Condens. Matter **14** (2002) 12311–12328 PII: S0953-8984(02)39743-1

Hyperfine fields and field gradients of thin films of face-centred-cubic Fe on Cu(001)

J A Gómez and Diana Guenzburger

Centro Brasileiro de Pesquisas Físicas, Rua Xavier Sigaud 150, 22290-180 Rio de Janeiro, RJ, Brazil

E-mail: gomez@cat.cbpf.br and diana@cat.cbpf.br

Received 19 July 2002
Published 15 November 2002
Online at stacks.iop.org/JPhysCM/14/12311

Abstract

The discrete variational method in density functional theory was employed to perform first-principles electronic structure calculations for embedded clusters representing thin films of face-centred-cubic Fe on a Cu(001) substrate. 3, 4 and 5 ML of Fe were investigated; the ferromagnetic and several types of antiferromagnetic spin configurations were considered. Layer-by-layer calculations of the contact and dipolar components of the magnetic hyperfine field are reported, as well as electric-field gradients at the surface and interface layers. Significant field gradients were found at the surfaces. Clusters modelling the interdiffusion of Fe and Cu between two layers at the interface were also investigated, to determine the effects on the properties.

1. Introduction

New materials with artificial structure have attracted great interest due to possible technological applications. Face-centred-cubic (fcc) Fe (or γ-Fe) is stable only at high temperatures ($\sim$1200 K), but may be obtained artificially at low or room temperature (RT), when precipitated or grown epitaxially on metals with fcc structure. In this manner it was possible to verify experimentally the complex relation between its structural and magnetic properties. First-principles electronic structure calculations have revealed that the latter are strongly related to the atomic volume, depending on which high or low spin ferromagnetic (FM) [1, 2] or antiferromagnetic (AFM) [2] phases have been predicted, as well as complex spiral magnetic structures [3, 4].

In particular, the system Fe/Cu(001) has been extensively investigated both experimentally [5–20] and theoretically [21–33] for more than a decade. Among the experimental methods employed are LEED (low-energy electron diffraction) [13–17, 20], RHEED (reflection high-energy electron diffraction) [14, 15], spin-polarized photoelectron emission [11], Mössbauer spectroscopy [5–10], EXAFS (extended x-ray absorption fine structure) [12], Kerr effect [13, 15, 16, 19, 20] and XMCD (x-ray magnetic circular

0953-8984/02/4712311+18$30.00

dichroism) [18]. One of the technological applications is to produce systems with ultrathin layers with the easy magnetization axis perpendicular to the surface, for the construction of magneto-optic devices [34–36]. Epitaxial growth of fcc Fe on Cu is favoured by the small difference in the lattice parameters and by the fact that the two metals are insoluble at RT.

The crystal structure and magnetic properties of the overlayers depend strongly on the conditions in which Fe is grown over Cu [7, 10]. The samples may be prepared at low or room temperatures. When they are prepared at RT, three regions may be identified, depending on the number of Fe monolayers (ML). In region I, from 1 to 4 or 5 ML Fe, the coupling among the latter is FM [6, 7, 9–11, 15, 16]; the structure is fct (tetragonal) [6, 7, 9, 10, 12, 15–17] with increase in the volume per atom to 12.1 Å^3 [16] and tridimensional lattice modulation [16, 17]. In region II, between $\sim$5 and $\sim$11 ML, below the surface Fe has fcc structure (on average) and atomic volume equal to γ-Fe (11.4 Å^3), AFM coupling and low total magnetic moment [5–7, 10, 15, 17]. In this region there is evidence of FM coupling between the surface and subsurface MLs [13, 19], followed by a tetragonal expansion between these two layers [16]. In both regions I and II the axis of easy magnetization is perpendicular to the surface [10, 13]. In region III, films thicker than 11 ML of fcc Fe are structurally unstable, and transform to bcc Fe with FM coupling between the layers and axis of easy magnetization in the ML plane [13, 17].

From the point of view of electronic structure calculations, recent first-principles band-structure calculations in density functional theory (DFT), including non-local corrections to the exchange–correlation energy (GGA), have been performed to search the spin configuration of the ground state, as well as calculating the relative energies of the lower-lying spin configurations, for regions I and II. Asada and Blügel [27] employed the full potential linear APW (FLAPW) method in film geometry combined with GGA to calculate the total energies for systems with 1–6 ML of fcc Fe over Cu(001) for all possible spin configurations, for the lattice constant of Cu. These authors found that 'all possible spin states exist and are stable or metastable states'. They obtained that for 2 and 3 ML of Fe, FM coupling is more stable; for a number of MLs greater than three, the AFM coupling of bilayers (++−−$\cdots$/Cu) (where the plus sign represents an Fe layer with positive spin) is the ground state configuration for an even number of MLs (four and six). For 5 ML of Fe, the ground state configuration is (++−−−/Cu), for which they also predict FM coupling between the surface and subsurface layers. For $n = 4$ and 5, the FM configuration is among the lowest energy states. Moroni *et al* [28, 29] calculated the total energies of films from 1 to 9 ML of Fe on Cu(001) employing the Vienna *ab initio* simulation package (VASP) with GGA; their results also predict an FM ground state for $n = 3$ and AFM coupling in the ground state for a number of MLs equal or greater than four. These authors obtained that for an even number of MLs the lower-energy spin configuration is AFM bilayers, the same as in [27]; for an odd number of MLs, there is a competition between different AFM configurations, but always with FM coupling between surface and subsurface layers, as well as at the Fe/Cu interface. For $n = 5$, the ground state is (++−−−/Cu), the same as in [27]. Furthermore, relaxation of the distances between layers was also taken into account (for the ground state spin configurations); the result obtained was that for 2 ML with FM coupling, the distance was slightly expanded with respect to the ideal epitaxial structure (lattice parameter of Cu), whereas AFM-coupled MLs were contracted.

Spišák *et al* [30] performed extensive total energy calculations for thin films with 1, 2, 4 and 6 ML of γ-Fe on Cu(001), taking into account lateral relaxation as well as between layers; they predict complex reconstruction which is dependent on the number of MLs and on the spin configuration. Their results agree partially with LEED measurements reported [17], with which they disagree regarding the interatomic distances. We may mention that theoretical calculations by Popescu *et al* [32], dedicated to interpreting experimental measurements by

spin-resolved appearance potential spectroscopy, lead to the conclusion by the authors that for 3 ML the ground state is AFM, contrary to the results of Asada and Blügel [27] and of Moroni *et al* [28, 29].

From these intensive theoretical and experimental efforts, a detailed microscopic picture of the *n*Fe/Cu system in regions I and II has emerged. However, one noticeable discrepancy between theory and experiment is the case of 4 ML, for which the former predicts AFM coupling, whereas the latter indicates FM.

Among the experimental techniques available to study the magnetism of these systems, Mössbauer spectroscopy is of great utility [5–10]. From measurements of the hyperfine field (HF) the magnetic phase may be determined, as well as the direction of magnetization. The magnetic phase transition temperature is determined by performing Mössbauer spectroscopy measurements at different temperatures. Furthermore, due to the local nature of Mössbauer measurements, the Mössbauer probe ^{57}Fe may be placed in a desired site. Thus, Keune and collaborators [7] used CEMS (conversion electron Mössbauer spectroscopy) to perform the first direct observation in 7Fe/Cu at 300 K that the FM configuration was restricted to the surface and the inner layers were in a paramagnetic phase. These inner layers present AFM coupling at low temperatures (45 K) [10].

In spite of the wealth of experimental data, very few reports are found on theoretical calculations of HF in *n*Fe/Cu overlayers and multilayers; to our knowledge, no calculations of electric field gradients (EFGs) have been performed. Freeman and collaborators [21, 22] performed band structure calculations with the FLAPW method for overlayers of Fe/Cu and obtained contact HFs; however, only 1 and 2 ML Fe were considered. Guo and Ebert [31] reported calculations of HF for periodic multilayers (superstructures) of Fe/Cu utilizing the spin-polarized relativistic LMTO method and considered, besides the contact contribution, the dipolar and orbital; these were also limited to 1 and 2 ML (FM) Fe.

Here we report results of first-principles electronic structure calculations in real space with the spin-polarized discrete variational method (DVM) [37, 38] in DFT [39] and the local spin-density approximation (LSDA), for films of fcc Fe on Cu(001). We obtained magnetic moments, HFs and EFGs. For the HF, we considered the contact (Fermi) and dipolar contributions, the latter only at the surface and interface layers.

The systems investigated were represented by clusters of atoms embedded in the potential of the external atoms in the solid. The same method was successfully applied to the calculation of HFs of fcc Fe [24] and particles of Fe in Cu [25]. Real-space cluster methods are appropriate for the calculation of local properties, such as magnetic moments and HF. We considered overlayers of Fe on Cu with the structure *n*Fe/2Cu, with $n = 3$, 4 and 5, in the FM spin configuration and some AFM configurations among the Fe ML. Each layer of Fe includes 12 or 13 atoms in the cluster, plus the surrounding atoms of the embedding on the same plane. The two layers of Cu with 12 or 13 atoms in the cluster, plus the Cu atoms of the embedding on the same plane and under, represent the Cu substrate. We also considered a model for the homogeneous interdiffusion between one Fe and one Cu layer at the Fe/Cu interface of the system 5Fe/Cu, represented by the cluster 4Fe/2(FeCu)/1Cu, for FM and one AFM configurations. Unless otherwise stated, calculations were performed for the lattice parameter of Cu ($a = 3.61$ Å); for the system 4Fe/2Cu, we performed calculations also for the tetragonally expanded fct structure, utilizing experimentally obtained distances among the layers [16].

A summary of some preliminary results has been published previously [40]. Preliminary results were given for 3Fe/Cu(001) in the FM and a hypothetical AFM spin configurations, and a qualitative discussion of the signs and magnitudes of the calculated HFs was presented, based on electron occupations of the orbitals.

This paper is organized as follows: in section 2, we describe briefly the theoretical method and give details of the present calculations; in section 3, we present and discuss our results. In section 4, we summarize our conclusions.

2. Theoretical method

The DVM has been described in the literature [37, 38]; here we give a brief summary of its main features. We seek the self-consistent-field (SCF) solutions of the Kohn–Sham one-electron equations of DFT [39] for the embedded clusters in a three-dimensional numerical grid, where the potential is a functional of the spin-dependent electron charge density $\rho_\sigma(\boldsymbol{r})$ obtained from the cluster spin–orbitals and the embedding. Here we employed the local exchange–correlation potential derived by Vosko *et al* [41], a parametrization of the simulations of Ceperley and Alder [42]. In the spin-polarized scheme, electron densities of different spins have the freedom to be different. The cluster orbitals are expanded as a linear combination of symmetrized atomic numerical orbitals (LCAO), obtained by atomic LSD SCF calculations. The spin density is given by $(\rho_\uparrow(\boldsymbol{r}) - \rho_\downarrow(\boldsymbol{r}))$, where the arrows represent the spin of the electron density.

A model density is employed to construct the cluster potential, which is an overlapping expansion in multipoles centred at the cluster nuclei [43]. This expansion is fitted to the 'real' density by least-squares minimization. In the present calculations, only $l = 0$ terms were considered, which is adequate to represent the electron densities of metals with compact structures. The convergence criterion for the SCF convergence was a difference $< 10^{-3}$ in the model density between two successive cycles. The central atom of each layer is where the calculations of the local properties are performed, since they are less affected by the lateral truncation of the clusters.

After the SCF procedure for the cluster is completed, a Mulliken-type population analysis [44], based on the coefficients of the LCAO expansion, is performed. This analysis roughly distributes the electrons among the atomic orbitals proportionally to their coefficients in the LCAO expansion; the overlap (crossed terms) populations are distributed proportionally to the coefficients of the atoms in the spin–orbital of the cluster. This analysis is very useful since it renders it possible to obtain approximately the occupations of the atomic orbitals of the atoms in the cluster. The orbitals included in the variational space were 3d, 4s and 4p for both Fe and Cu. The inner (core) orbitals were considered 'frozen' after the first iteration, when they are explicitly orthogonalized to the orbitals of the valence.

Atomic charges and magnetic moments are obtained by integrating the electron charge density $\rho(\boldsymbol{r})$ or spin density $(\rho_\uparrow(\boldsymbol{r}) - \rho_\downarrow(\boldsymbol{r}))$ inside the Wigner–Seitz volume of the atom.

We considered four classes of embedded clusters to represent the Fe/Cu interface: 3Fe/2Cu, 4Fe/2Cu, 5Fe/2Cu and 4Fe/2(FeCu)/1Cu. The first three represent 3, 4 and 5 ML of Fe grown epitaxially over a fcc Cu(001) substrate, the latter represented by 2 ML of Cu. Each Fe ML contains 12 or 13 atoms in the cluster, plus the surrounding atoms of the embedding in the same plane. An example of a cluster is shown in figure 1. The system 4Fe/2(FeCu)/1Cu represents the homogeneous interdiffusion at the Fe/Cu interface of 5Fe/2Cu, which produces an homogeneous alloy 2 ML thick. Unless otherwise stated, the lattice parameter of Cu was used in the calculations ($a = 3.61$ Å).

Here the DVM embedding scheme, originally designed for clusters in the bulk, was adapted for the bidimensional cases considered. The clusters are embedded in the potential generated by the electronic density and the nuclei of approximately 1500 external atoms in the solid. The electronic density of the external atoms is obtained with LSDA atomic calculations; to avoid spurious migration of cluster electrons to the external atoms, their potentials are truncated at -0.3 Hartrees inside a radius of 2.0 au centred at the nucleus. The total set (cluster + atoms

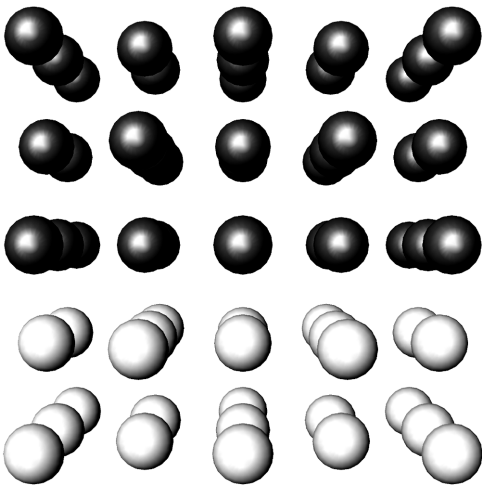

Figure 1. Representation of the cluster 3Fe/2Cu. The dark spheres represent Fe atoms; light spheres represent Cu.

of the embedding) formed a cylinder with radius ∼30 au, consisting of MLs of Fe and Cu. The atoms of the cluster, which are the ones that take part in the variational calculation, were placed at the top central position inside the cylinder. One of the bases of the cylinder contains the Fe atoms (cluster + embedding) pertaining to the Fe surface, therefore above this layer is the vacuum. To model the Cu crystal we included a total of 10 MLs, but only the first two, starting from the interface, contain Cu atoms pertaining to the cluster. In each layer, the atoms of the embedding were polarized in the same way as those of the cluster, depending on the magnetic configuration considered. Furthermore, electron configurations and magnetic moments considered in generating the electronic densities of the atoms of the embedding were made approximately equal to those obtained for the cluster with a Mulliken population analysis, after a preliminary set of iterations. As mentioned before, local properties were calculated at the central atom of the 13-atom layers. For 4Fe/2Cu, the cluster surface layer consisted of 12 atoms, with none at the centre; therefore, it was expanded to 16 atoms, and local properties were calculated at the innermost atoms, placed at $(1/2)a$ from the centre.

In the following table are given the number of cluster atoms:

System	Fe	Cu	Total
3Fe/2Cu	38	25	63
4Fe/2Cu	54	25	79
5Fe/2Cu	63	25	88
4Fe/2(FeCu)/1Cu	65	23	88

The following notation for the Fe layers is employed: the surface ML is denoted S, the next ML in $S-1$, and so on. The interface is denoted I. For the system where there is interdiffusion between the I ML of Fe and the first ML of Cu, the latter will be denoted $I-1$.

Finally, we also considered the system 4Fe/2Cu FM with distances between the MLs as determined by LEED [16], that is, with average tetragonal expansion relative to the same distance in Cu (1.805 Å). The distances are 1.78, 1.85, 1.90 and 1.86 Å, from the interface to the surface. This system will be denoted 'fct' hereafter.

3. Results and discussion

As mentioned in the introduction, theoretical determinations of the relative energies of the spin configurations of the overlayers nFe/Cu ($n = 3$–5) with ideal interface, with first-principles methods and gradient corrections to the exchange–correlation energy, have been recently reported [27–29]. We have thus used these results for guidance for which spin states we performed our calculations.

It was demonstrated theoretically that for $n = 3$–6 all possible spin states exist and are stable or metastable states [27]. Furthermore, from the extensive experimental literature on Fe films on Cu, it has become clear that different experimental conditions of sample preparation, temperature etc may result in different spin arrangements.

In this work we included the FM configuration among all the MLs in all cases (nFe/2Cu, $n = 3$–5) since, according to theoretical calculations, it either has the lowest energy ($n = 3$) or is among the lowest energy spin configurations [27–29]. In addition, we included some lowest energy AFM configurations. From the energy calculations [27–29], it is seen that even for AFM configurations stability is favoured by FM coupling of the surface bilayers.

For all spin configurations we considered that the atoms in the same layer are all coupled ferromagnetically, as is generally assumed, including in other theoretical calculations where the energetics was investigated; however, the possibility of more complex intralayer spin configurations cannot be entirely ruled out [15].

3.1. Charges, magnetic moments and hyperfine fields

In the first column of table 1 are given the charges Q of the Fe atoms of each layer, which are defined as the atomic number Z minus the integral of the electron charge density inside the Wigner–Seitz volume of the atom. The spin states of the layered systems are represented by $(+++\cdots)$, etc, where the positive (negative) sign represents positive (negative) spin on the Fe layer, from the surface (left) to the interface (right). We adopted the convention that the Fe spin at the interface layer is always positive. The Fe charges thus defined are very small, being somewhat larger only at the surface layers, at the interface layers of 5Fe/2Cu and at the mixed Fe–Cu layers of 4Fe/2(FeCu)/1Cu. Most of the charges are positive. The largest positive charges are at the surface; positive charges at the surface in overlayers of Fe on Cu have been obtained before in calculations with the KKR method [26]. The Fe atoms that are in contact with Cu also have small positive charges in almost all cases (layers I in nFe/2Cu, I and $I - 1$ in 4Fe/(2(FeCu)/1Cu); correspondingly, Q of the interface Cu atoms have small negative values (not shown in the table). This is evidence of Fe $\rightarrow$ Cu charge transfer at the interface, which may be understood since the electronegativity of Cu is slightly larger than Fe.

The second column of table 1 shows the spin magnetic moments μ of the Fe atoms of each layer, defined as the integral of the spin density $(\rho_\uparrow(\boldsymbol{r}) - \rho_\downarrow(\boldsymbol{r}))$ inside the Wigner–Seitz cell. In all cases, the magnetic moments at the surface are larger than at the inner layers. Values at the surface are very similar regardless of the number of Fe layers, and vary between 2.81 and 2.89 μ_B. Similar values at the surface were found for Fe overlayers in calculations with a pseudo-potential band-structure method [28, 29]. The increase of the magnetic moments at the surface may be ascribed to the truncation of the d–d bonds at the surface and consequent localization of the states, producing a narrowing of the bands. Thus the Fe at the surface becomes more similar to the free atom, which has $\mu = 4\ \mu_B$. As an example, we show in figure 2 the local density of states (DOS) of 5Fe/2Cu FM, where we may see a narrowing of the valence bands of Fe at the surface layer, relative to the inner layer $S - 2$ and interface I. This results in depletion of the spin down band at the surface and consequent increase of the moment.

Table 1. Charge Q, magnetic moment μ (in μ_B), contact HF of the core B_c^{core}, valence contact HF B_c^{val} and total contact HF B_c (in T) and perpendicular ($B_\perp^D$) and parallel ($B_\parallel^D$) components of the dipolar field (in T) of Fe in the ML. Q is defined as the integral of the charge density (including the nuclear charge) inside the Wigner–Seitz cell pertaining to the atom. μ is defined as the integral of the electron spin density inside the Wigner–Seitz cell. (∗) Theoretical spin ground state [27–29]. (+) Experimental spin ground state [16]. (#) Experimental spin ground state [7, 10, 16].

System	Spin config.	Layer	Q	μ	B_c^{core}	B_c^{val}	B_c	$B_\parallel^D$	$B_\perp^D$
3Fe/2Cu	(+++)	S	0.12	+2.89	−28.5	+4.4	−24.1	−1.6	+3.2
	(∗) (#)	$S-1$	0.01	+2.41	−24.8	−7.4	−32.2		
		I	0.01	+2.37	−24.0	−0.4	−24.4	−0.3	+0.6
	(−−+)	S	0.12	−2.88	+28.3	−5.5	+22.8	+1.4	−2.7
		$S-1$	0.01	−2.17	+21.9	−1.3	+20.7		
		I	0.01	+2.09	−21.1	+6.3	−14.8	−0.3	+0.5
4Fe/2Cu	(++++)	S	0.10	+2.85	−28.3	+1.7	−26.6	−1.4	+2.8
	(+)	$S-1$	−0.05	+2.22	−22.9	−7.9	−30.8		
		$S-2$	0.02	+2.36	−24.2	−6.0	−30.2		
		I	0.00	+2.42	−24.5	−1.0	−25.5	−0.15	+0.3
	(++++)	S	0.09	+2.86	−28.5	+1.5	−27.0	−1.4	+2.7
	fct (+)	$S-1$	−0.03	+2.36	−24.4	−7.3	−31.7		
		$S-2$	0.01	+2.44	−25.0	−6.0	−31.0		
		I	−0.01	+2.40	−24.3	−1.3	−25.6	−0.1	+0.2
	(−−++)	S	0.10	−2.83	+28.1	−3.4	+24.7	+1.1	−2.1
	(∗)	$S-1$	−0.05	−1.92	+19.6	+0.4	+20.0		
		$S-2$	0.01	+2.04	−20.8	+1.5	−19.4		
		I	0.00	+2.38	−24.2	−0.2	−24.4	+0.1	−0.2
5Fe/2Cu	(+++++)	S	0.13	+2.85	−28.1	+2.8	−25.3	−1.6	+3.2
		$S-1$	−0.01	+2.41	−24.8	−7.6	−32.4		
		$S-2$	−0.02	+2.13	−22.0	−6.0	−28.0		
		$S-3$	0.02	+2.43	−25.0	−6.4	−31.4		
		I	0.06	+2.44	−24.7	−1.8	−26.5	−0.3	+0.6
	(−−+++)	S	0.12	−2.85	+28.1	−5.6	+22.5	+1.2	−2.4
	(∗)	$S-1$	−0.02	−2.19	+22.3	−1.4	+20.9		
		$S-2$	−0.02	+1.92	−19.5	+1.5	−18.0		
		$S-3$	0.02	+2.39	−24.5	−5.7	−30.2		
		I	0.06	+2.41	−24.5	−2.2	−26.7	−0.05	+0.1
	(−−−++)	S	0.13	−2.82	+27.9	−0.5	+27.4	+1.4	−2.8
		$S-1$	−0.01	−2.38	+24.5	+7.0	+31.5		
		$S-2$	−0.02	−1.83	+18.6	−1.7	+16.9		
		$S-3$	0.01	+2.20	−22.4	+2.1	−20.3		
		I	0.06	+2.45	−24.8	+0.0	−24.8	+0.15	−0.3
	(++−++)	S	0.13	+2.85	−28.0	+6.1	−21.9	−1.5	+2.9
		$S-1$	−0.01	+2.17	−22.0	+0.9	−21.1		
		$S-2$	−0.02	−1.77	+18.0	−9.2	+8.8		
		$S-3$	0.01	+2.17	−22.0	+1.7	−20.3		
		I	0.06	+2.45	−24.8	+0.5	−24.3	−0.1	+0.2
4Fe/2(FeCu)/	(++++++)	S	0.11	+2.85	−28.0	+2.6	−25.4	−1.6	+3.3
1Cu		$S-1$	0.00	+2.40	−24.6	−7.5	−32.1		
		$S-2$	−0.05	+2.15	−22.0	−5.5	−27.5		
		$S-3$	0.02	+2.41	−24.7	−4.6	−29.3		
		I	0.06	+2.37	−24.0	+0.1	−24.1	+0.2	−0.5
		$I-1$	0.19	+2.49	−25.3	+4.1	−21.2		

Table 1. (Continued.)

System	Spin config.	Layer	Q	μ	B_c^{core}	B_c^{val}	B_c	$B_\parallel^D$	$B_\perp^D$
	$(--++++)$	S	0.10	−2.81	+27.6	−5.6	+22.0	+1.3	−2.5
	$(*)$	$S-1$	−0.01	−2.06	+21.0	−0.9	+20.1		
		$S-2$	−0.04	+1.96	−20.0	+1.9	−18.1		
		$S-3$	0.03	+2.38	−24.5	−3.8	−28.3		
		I	0.06	+2.33	−23.7	−0.5	−24.2	+0.5	−1.0
		$I-1$	0.19	+2.48	−25.2	+4.2	−21.0		

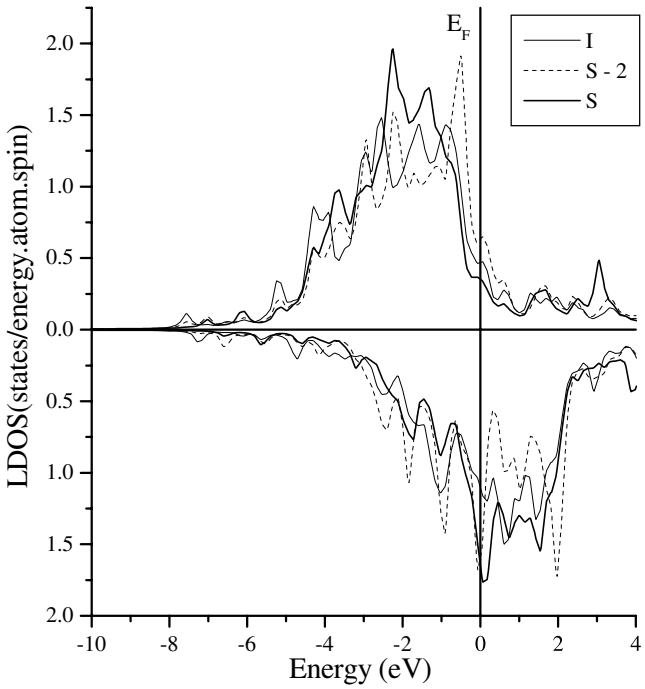

Figure 2. Local density of states (LDOS) of the valence orbitals 3d + 4s+ 4p of Fe in the layers I, $S-2$ and S of 5Fe/2Cu in the FM spin configuration. The LDOS is obtained by broadening the discrete cluster energy levels with Lorentzians [38]. Positive spin states are in the upper section of the figure.

In all cases, we observe that whenever there is AFM coupling between two layers, the moments of the Fe atoms in these layers are considerably reduced, with respect to the same layers in the FM configuration.

For FM 4Fe/2Cu, there is only a small difference between the values of the moments obtained in the ideal fcc structure, with the lattice parameter of Cu, and the values for the tetragonally distorted structure (fct), calculated with the experimental distances obtained by LEED measurements in the spin ground state, determined to be FM by SMOKE [16]. For the latter fct structure, we see that the moment at the interface is slightly smaller due to a smaller Fe–Cu distance (see section 2), whereas for the other layers there is an increase of the moment due to increased distances among the layers.

The HF was calculated for each Fe ML. The contact or Fermi contribution to the HF is defined as [45]

$$B_c = 8/3\pi\mu_B[\rho_\uparrow(0) - \rho_\downarrow(0)] \tag{1}$$

where μ_B is the Bohr magneton. For the calculation of B_c, only the contribution of the valence electrons B_c^{val} was calculated with the spin density $(\rho_\uparrow(0) - \rho_\downarrow(0))$ obtained from the SCF cluster calculations; the contribution of the electrons in the core orbitals (1s, 2s and 3s in the non-relativistic approximation) B_c^{core} was obtained from atomic DFT calculations, for Fe with the electron configurations as obtained with the Mulliken populations analysis, after the SCF iterations for the cluster (for example, $3d_\uparrow^{4.88}4s_\uparrow^{0.34}4p_\uparrow^{0.16}$ $3d_\downarrow^{2.02}4s_\downarrow^{0.27}4p_\downarrow^{0.15}$ for the S layer of FM 3Fe/2Cu). The dipolar contribution was calculated only at the surface and interface layers, where a non-negligible anisotropy of the spin density is expected, and is determined by the expression [45]

$$B_{ij}^D = 1/2 g_e \mu_B \int [\rho_\uparrow(\boldsymbol{r}) - \rho_\downarrow(\boldsymbol{r})](3x_i x_j - \delta_{ij} r^2)/r^5 \, \mathrm{d}\boldsymbol{r}, \tag{2}$$

where B_{ij}^D are the components of the dipolar HF tensor and x_i, $x_j = x, y, z$. The dipolar HF tensor is traceless and, in the present case, diagonal by symmetry.

In table 1 are shown the values of the contact HF of the core B_c^{core}, valence contact field B_c^{val} and total B_c, and the components of the dipolar field parallel $B_\parallel^D$ and perpendicular $B_\perp^D$ to the plane of the ML. We observe that the most significant contribution to the contact HF comes from the core electrons, independently of the spin configuration. The sign of the core contribution is always opposite to that of the 3d moment. This is due to the well known spin polarization of the core electrons by the 3d moment, which 'attracts' electrons of the same spin by way of the exchange interaction, leaving a net density of opposite spin at the nucleus. In figure 3 are plotted the values of B_c^{core} against μ, showing the well known proportionality between magnetic moments and the magnitude of the core HF. A linear fit of the data gave a coefficient equal to $-9.15\,\mathrm{T}\,\mu_B^{-1}$. A similar number was obtained recently in calculations with the same method for Co particles in Cu ($-9.3\,\mathrm{T}\,\mu_B^{-1}$) [46]. Guo and Ebert [31] obtained a similar linear relation for multilayers of Fe and Co, but with a coefficient of somewhat greater magnitude ($-11.3\,\mathrm{T}\,\mu_B^{-1}$), probably due to the inclusion of relativistic effects which are significant for the core electrons, since they have high kinetic energy. In contrast to the core 1s–3s electrons, the spin density at the Fe nucleus of the valence (conduction) electrons may either have the same sign as the 3d moment, or opposite sign, depending on the polarization induced by μ(3d) on these electrons.

For the FM spin configurations, we observe that the magnitude of the contact HF is generally larger in the intermediate layers, with respect to the surface and interface. At the interface layers, the contribution of the valence electrons B_c^{val} is small and negative. For the intermediate layers, the contribution of the valence electrons is significant and negative, and at the surface it is significant and positive. The large negative values of the valence contributions B_c^{val}, added to the negative values of the core contributions, result in large negative total values of B_c at the intermediate layers. The same was obtained for FM bulk fcc Fe, in calculations with the same method [24, 25]. Inversely, at the surface layers the large positive values of the valence contributions, added to the negative core contributions, reduce significantly the magnitude of the total contact HF B_c. This explains why, although the magnetic moment is larger at the surface, the magnitude of the HF is smaller than at the inner layers. As for the interface, the smaller magnitude of B_c is mainly due to a smaller μ.

Comparing the values of B_c for 4Fe/2Cu in the fcc and in the fct structures of Fe in the FM configuration, we see in table 1 that the changes brought on by the tetragonal distortion are small, as are the changes of the magnetic moments. These changes in B_c are larger for the two inner layers, where the magnitudes of B_c have increased from fcc to fct due to slightly increased magnetic moments.

For the AFM spin configurations, as mentioned before the magnetic moments at Fe layers coupled antiferromagnetically are reduced. This results in smaller magnitudes of B_c^{core} at these

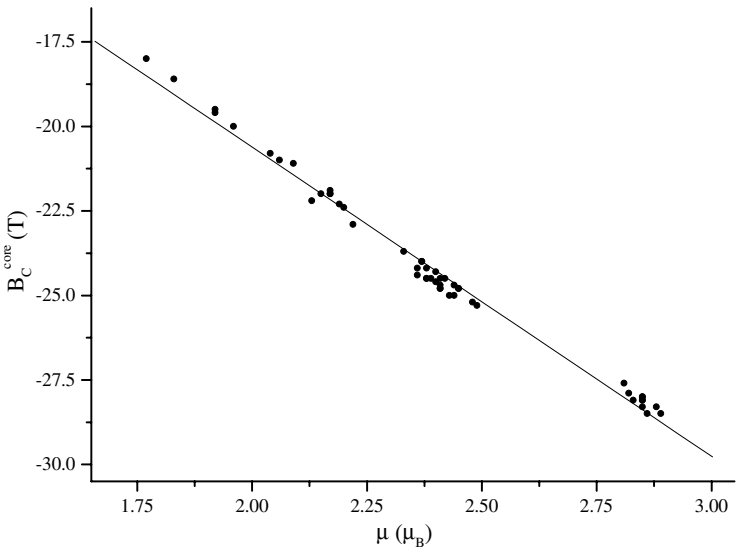

Figure 3. Plot of the core HFs B_c^{core} of Fe against magnetic moments μ for nFe/2Cu ($n = 3$–5) and 4Fe/2(FeCu)/1Cu. The straight line is the result of a linear fit, with proportionality constant -9.15 T μ_B^{-1}.

layers. Furthermore, as was obtained in calculations for bulk AFM fcc Fe [24], the sign of B_c^{val} for these inner layers with AFM coupling is practically always opposite to B_c^{core}. These two factors result in considerably reduced magnitudes of B_c at the layers with AFM coupling (see table 1). For a ML with AFM coupling with two adjacent layers, the reduction of the magnitude of B_c is even more pronounced, as is the case for the $S-2$ layer in the (++−++) configuration of 5Fe/2Cu ($B_c = 8.8$ T). On the other hand, in some AFM spin configurations there may exist layers with FM coupling to two adjacent MLs; in such a case, $|B_c|$ may be high, due to the local environment being FM, and thus the valence and core contributions having the same sign. As an example of the latter case, see layer $S-1$ of configuration (−−−++) of 5Fe/2Cu ($B_c = 31.5$ T).

In summary, the main component of the HF which is B_c is seen to have quite an extended range of magnitudes in the different layers. This may account for the broad peaks of HF distribution found experimentally [7]. In general, we may say that the magnitude of B_c is reduced by AFM coupling among layers. The valence (or conduction electron) contribution B_c^{val} may or may not have the same sign as the core contribution B_c^{core}; since the magnitude of the latter is always proportional to the spin magnetic moment μ, it is concluded that no proportionality between the magnitude of the total field B_c and μ is to be expected.

In table 1 it is seen that the dipolar HF has non-negligible values at the interface and surface layers, specially at the latter, with the principal component in the direction perpendicular to the plane of the ML. In table 2 are tabulated the values of B_c, the perpendicular and parallel components of the dipolar field ($B_\perp^D$ and $B_\parallel^D$ respectively) and the resulting total HF in both directions, for the surface Fe layer. We observe that the sign of the perpendicular dipolar field is always opposite to that of B_c, thus reducing the magnitude of the total field in this direction. Inversely, the parallel component has the same sign as B_c, and thus enhances the total HF in the parallel direction. These results may be relevant for the determination of the direction of magnetization from experimental HF values. The relativistic calculations of [31] for FM

Table 2. Contact HF B_c, perpendicular ($\perp$) and parallel ($\parallel$) components of the dipolar field B^D and total HF B (in T) at the Fe surface layers. ($*$) Theoretical spin ground state [27–29]. (+) Experimental spin ground state [16]. (#) Experimental spin ground state [7, 10, 16].

System	Spin config.	Direction of magnetization	B_c	B^D	B
3Fe/2Cu	(+++)	$\perp$	−24.1	+3.2	−20.9
	(∗) (#)	$\parallel$	−24.1	−1.6	−25.7
	(−−+)	$\perp$	+22.8	−2.7	+20.1
		$\parallel$	+22.8	+1.4	+24.2
4Fe/2Cu	(++++)	$\perp$	−26.6	+2.8	−23.8
	(+)	$\parallel$	−26.6	−1.4	−28.0
	(++++)	$\perp$	−27.0	+2.7	−24.3
	fct (+)	$\parallel$	−27.0	−1.4	−28.4
	(−−++)	$\perp$	+24.7	−2.1	+22.6
	(∗)	$\parallel$	+24.7	+1.1	+25.8
5Fe/2Cu	(+++++)	$\perp$	−25.3	+3.2	−22.1
		$\parallel$	−25.3	−1.6	−26.9
	(−−+++)	$\perp$	+22.5	−2.4	+20.1
	(∗)	$\parallel$	+22.5	+1.2	+23.7
	(−−−++)	$\perp$	+27.4	−2.8	+24.6
		$\parallel$	+27.4	+1.4	+28.8
	(++−++)	$\perp$	−21.9	+2.9	−19.0
		$\parallel$	−21.9	−1.5	−23.4
4Fe/2(FeCu)/1Cu	(++++++)	$\perp$	−25.4	+3.3	−22.1
		$\parallel$	−25.4	−1.6	−27.0
	(−−++++)	$\perp$	+22.0	−2.5	+19.5
	(∗)	$\parallel$	+22.0	+1.3	+23.3

periodic bilayers of Fe in Cu $(2\text{Fe}/6\text{Cu})_n$ also resulted in a dipolar HF with principal component perpendicular to the plane of the ML, and with opposite sign to B_c; the orbital component of HF was also calculated, and is of the order of 3 T in both directions. It must be mentioned that the present non-relativistic calculations do not include the orbital component of the HF, due to the absence of spin–orbit coupling. Although for metals they should be small, due to 'quenching' of the orbital moment, one may expect non-negligible values at the surface and interface.

In figures 4 and 5 are depicted the contour maps of the spin density for FM 5Fe/2Cu and 5Fe/2Cu with configuration (−−+++) respectively, in which we observe considerable spin anisotropy at the surface; this is the origin of the dipolar HF. We may see in both cases in the interstitial region the spin density of the Fe conduction electrons (4s and 4p), which has always opposite sign to the (more compact) spin density of the 3d. The polarization of the Cu atoms at the interface is also evident, with small induced 3d moments parallel to the Fe 3d.

So far we have discussed the overlayer systems nFe/2Cu ($n = 3$–5) with an ideal Fe–Cu interface; however, it is known that experimentally this condition is very difficult to achieve. The formation of an Fe–Cu alloy in the first layer of Fe on Cu was observed in films of 4 ML [7]; in films with 11 and 17 ML, an interdiffusion of up to 4 ML at the interface was reported [5]. To model this situation, we treated a system with a homogeneous interdiffusion of Fe and Cu occurring between the atoms of two layers, the Fe and Cu layers at the interface. We considered the I (Fe) and $I-1$ (Cu) layers of 5Fe/2Cu, and constructed a homogeneous mixture among the two layers by diffusing Fe atoms from I to $I-1$, and Cu atoms from $I-1$ to I, such that at

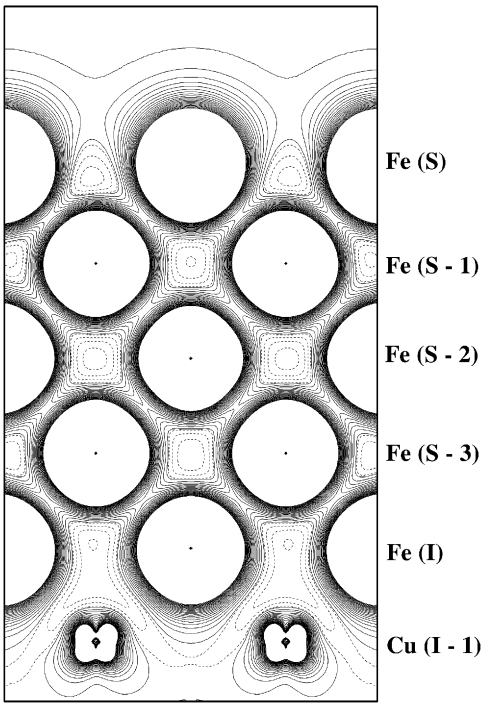

Figure 4. Contour map of the spin density $(\rho_\uparrow(\boldsymbol{r}) - \rho_\downarrow(\boldsymbol{r}))$ in a plane perpendicular to the layers for FM 5Fe/2Cu. Contours vary from -0.01 to -0.0001 with intervals $4.95 \times 10^{-4}\ e/a_0^3$, and from 0.0001 to 0.01 with intervals $4.95 \times 10^{-4}\ e/a_0^3$. Solid lines are positive values; dotted lines are negative values.

the I and $I - 1$ ML the Fe atoms are surrounded by Cu and vice versa, like two chess boards.

A similar model of interdiffusion for 4.5Fe/Cu was considered by Asada and Blügel [27], which they called 'checkerboard structure'. In their model, only one ML at the interface is mixed Fe and Cu; our model is more complete, since it considers interdiffusion among two MLs (Fe and Cu) at the interface. In their calculations, no significant effect of the interdiffusion on the relative energies of the different spin configurations was observed.

In general, the results of the HF obtained for 5Fe/2Cu also apply to the interdiffusion model system 4Fe/2(FeCu)/1Cu. Only the spin configurations FM and $(--+++)$ were investigated, the latter found to be the spin ground state in theoretical calculations for the ideal interface [27–29]. The results are also given in tables 1 and 2. It is seen that only at the mixed layers I and $I - 1$ are the results significantly different; for the upper layers the values converge rapidly to those of the model with the ideal interface. For the surface layer, they are practically identical, as may be observed in table 2. Comparing 4Fe/2(FeCu)/1Cu with 5Fe/2Cu in table 1, we observe a larger positive charge on Fe in layer $I - 1$ of the former. The mixture with the Cu atoms in layers I and $I - 1$ has also the effect of reducing the magnitude of B_c of Fe in these layers. In layer $I - 1$ this is caused by a significant increase in B_c^{val}, with sign opposite to B_c^{core}. In figure 6 is depicted the spin density in the plane of layer I of 4Fe/2(FeCu)/1Cu. In this plane are also evident the small induced 3d moments of Cu, coupled ferromagnetically to the 3d moments of Fe. The negative spin density of the conduction electrons (4s and 4p) is seen in the interstitial region, surrounding both Fe and Cu atoms.

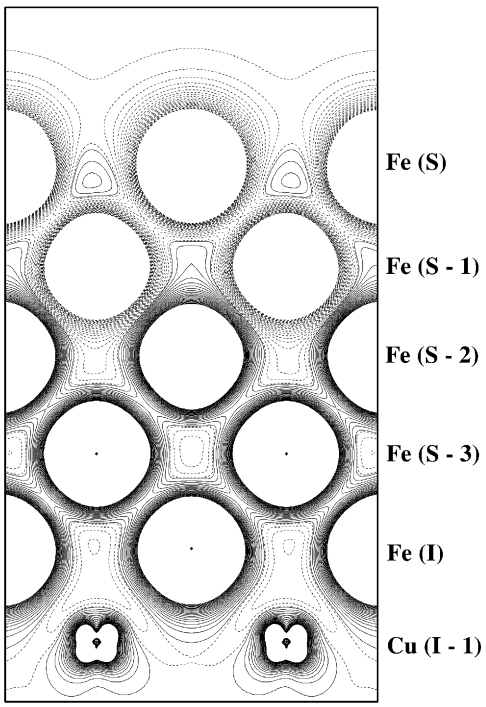

Figure 5. Contour map of the spin density in a plane perpendicular to the layers for 5Fe/2Cu with spin configuration (−−+++). Contour specifications as in figure 4.

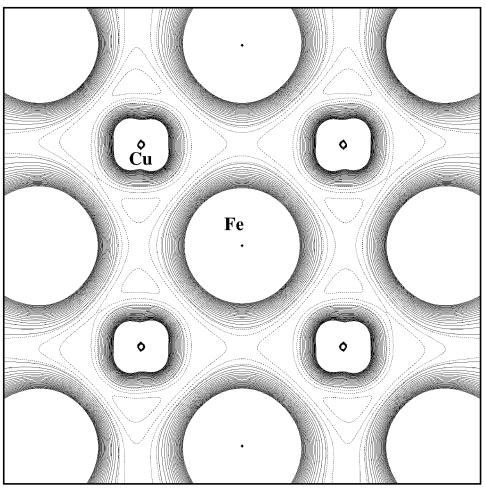

Figure 6. Contour map of the spin density in a plane containing the nuclear sites of the *I* layer of 4Fe/2(FeCu)/1Cu in the FM spin configuration. Contour specifications as in figure 4.

3.2. Electric-field gradients

The components V_{ij} of the EFG tensor at an Fe nucleus are given by (in au) [47]:

$$V_{ij} = -\int \rho(\boldsymbol{r})(3x_i x_j - \delta_{ij} r^2)/r^5 \,\mathrm{d}\boldsymbol{r} + \sum_q Z_q^{eff}(3x_{qi}x_{qj} - \delta_{ij} r_q^2)/r_q^5. \qquad (3)$$

Table 3. Calculated EFGs V_{zz} of Fe at the surface (S) and interface (I and $I-1$) layers of nFe/2Cu (n = 1–3) and 4Fe/2(FeCu)/1Cu. (∗) Theoretical spin ground state [27–29]. (+) Experimental spin ground state [16]. (#) Experimental spin ground state [7, 10, 16].

System	Spin config.	V_{zz} (10^{17} V cm^{-2})		
		S	I	$I-1$
3Fe/2Cu	(+++) (∗) (#)	5.17	1.85	—
	(−−+)	5.33	2.53	—
4Fe/2Cu	(++++) (+)	5.01	0.41	—
	(++++) fct (+)	5.08	0.32	—
	(−−++) (∗)	5.11	0.58	—
5Fe/2Cu	(+++++)	4.80	1.27	—
	(−−+++) (∗)	5.17	1.52	—
	(−−−++)	4.97	1.73	—
	(++−++)	5.13	1.68	—
4Fe/2(FeCu)/1Cu	(++++++)	4.72	−2.04 ($\eta = 0.97$)	1.61 ($\eta = 0.86$)
	(−−++++) (∗)	5.08	1.83 ($\eta = 0.89$)	1.63 ($\eta = 0.89$)

In equation (3), the first term is the electronic contribution of the valence electrons and the second term is the contribution of the surrounding nuclei, where Z_q^{eff} is the atomic number Z of atom q minus the number of core electrons. After diagonalization, the diagonal elements are redefined according to the convention $|V_{zz}| > |V_{yy}| \geqslant |V_{xx}|$.

The asymmetry parameter η is defined as

$$\eta = (V_{xx} - V_{yy})/V_{zz}. \tag{4}$$

According to the convention cited above, we see that $0 \leqslant \eta \leqslant 1$. With tetragonal symmetry around the probe atom, $\eta = 0$; the principal component V_{zz} is denoted EFG.

In table 3 are displayed the values of V_{zz} for the surface (S) and interface (I) layers of Fe in nFe/2Cu (n = 3–5), which are all positive and with direction perpendicular to the plane of the layers. For these cases with ideal interface, there is always tetragonal symmetry around the probe atom, and thus $\eta = 0$. We may see that the values at the surface are significantly larger than at the interface.

The large positive values at the surface may be explained as follows: the Fe in-plane orbitals $4p_x$, $4p_y$, $3d_{x^2-y^2}$ and $3d_{xy}$, which give positive contributions to the EFG [47], are more 'compressed', due to Pauli repulsion (orthogonality effects), and thus have an enhanced electron density near the nucleus, as compared to the orbitals $4p_z$, $3d_z^2$, $3d_{xz}$ and $3d_{yz}$ (z being the direction perpendicular to the ML), which give a negative contribution. An electron density $\rho(\boldsymbol{r})$ enhanced in the nuclear region increases the EFG due to the r^{-3} factor in equation (3). A similar interpretation was given for the origin of the positive EFG in calculations for Cd impurities in the surface of Cu and Ag [48].

In figure 7 is shown a contour map of the electron density $\rho(\boldsymbol{r})$ for FM 4Fe/2Cu; we may observe the considerably larger charge anisotropy at the surface, where the electronic charge density is free to expand outwards in the z direction. As explained previously, this is the origin of the large positive EFG at the surface. The other overlayer model systems give similar results.

For the calculations of V_{zz}, only the valence electrons were considered, since the core electrons were 'frozen' in the SCF procedure. It is known that the distortion of the valence electron charge distribution polarizes the core electrons, especially the Fe 3s and 3p (sometimes called 'shallow core' or 'semi-core'), creating a contribution to the EFG at the nucleus. Blaha *et al* [49] included the contribution of the semi-core in calculations of the EFG of hcp transition

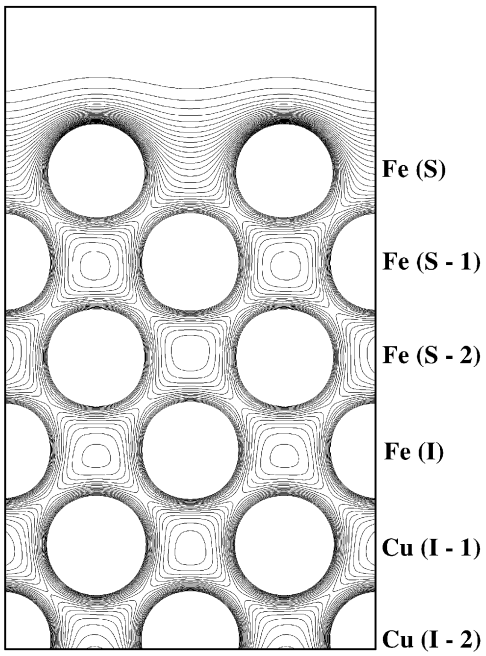

Figure 7. Contour map of the electron charge density $\rho(\boldsymbol{r})$ in a plane perpendicular to the layers for FM 4Fe/2 Cu. Contours vary from 0.0 to 0.06 with intervals $2.00 \times 10^{-3}\ e/a_0^3$.

metals and found it to be small (7% or less of the total). However, this percentage could be higher in the case of thin films, especially at interfaces and surfaces, where a larger charge anysotropy around the probe nucleus is present. In this case, the EFG values may be expected to have larger magnitudes than in bulk noncubic metals, and thus the semi-core polarization may be more important.

Table 3 shows also the values of the EFG on Fe for the model interdiffusion system 4Fe/2(FeCu)/1Cu. The largest values of V_{zz} are also found at the surface, with direction perpendicular to the ML. In this model for interdiffusion, the tetragonal symmetry around Fe is broken at the interface layers I and $I-1$ and thus $\eta \neq 0$. For the FM configuration, we obtained V_{zz} with a negative sign in the I layer, with direction perpendicular to the ML; in the $I-1$ layer the field gradient is positive and on the ML plane. For the spin configuration ($--++++$), for both I and $I-1$ the field gradient is positive and on the ML plane.

The values of $|V_{zz}|$ at the interface of the FM states are of the order of the value $+1.4 \times 10^{17}$ V cm^{-2} measured by Keune *et al* [7] in FM films with $\geqslant 3$ ML with ^{57}Fe Mössbauer spectroscopy. In those samples, interdiffusion at the interface is likely to have occurred; the authors estimate that it is limited to the first atomic Fe layer, as in our theoretical model. However, to our knowledge no experimental determinations of the EFG at the fcc Fe surface layers have been reported. Since we found these to be considerable, they should be taken into account when fitting the Mössbauer spectra.

3.3. Comparison with experimental magnetic moments and HF

Direct comparison with experimental results of magnetic moments, HF and EFG in films is not easy. In fact, the electronic structure calculations are able to give results for Fe in each ML individually, whereas in reported experimental determinations this separation is frequently not

possible. In this case, theory is able to give more detailed information and to make predictions on the individual layers. Furthermore, in general the exact spin state is not known in the experiments, and results depend on conditions of sample preparation, assumptions made when fitting the spectra, temperature of measurement etc. For Fe overlayers, the possibility of several different AFM spin configurations complicates things further.

Schmitz *et al* [50] reported values of magnetic moments in high-spin FM 3Fe/Cu(100) overlayers, obtained with magnetic circular dichroism in x-ray absorption spectroscopy (MCXD). They obtained an average value for the magnetic moment of 2.8 μ_B, which compares very well with 2.6 μ_B, our average of μ over the 3 Fe ML in FM 3Fe/2Cu (see table 1).

Dunn *et al* [51] reported similar measurements for 3.4 and 3.8 ML and obtained spin magnetic moments as high as 3.33 and 3.46 μ_B, respectively, for these samples (error $< 20\%$). Our calculations do not confirm such high values.

Keune *et al* [7] reported the distribution of HF values for FM samples of 3Fe/Cu(001) overlayers. The value of HF at the maximum peak in the distribution, for the sample prepared at 300 K, is 33.8 T (extrapolated to $T = 0$ K); for the sample prepared at 90 K, this value is 31.5 T. These may be compared with the magnitude of our calculated HF (32.2 T) at the intermediate layer ($S - 1$) in FM 3Fe/2Cu (see table 1). In the experimental distribution of HF are seen shoulders on the lower-magnitude side of the highest peak, which may be assigned to the surface and interface layers, for which our calculations found values of smaller magnitudes ($\sim$20–25 T; see tables 1 and 2).

Very recently, a multiple technique approach including the magneto-optical Kerr effect (MOKE) has been used to determine the magnetic structure of Fe films on Cu(001) [52]. It was demonstrated that Fe films with 6–9 MLs, except for the top two FM layers at the surface, have a spin-density-wave AFM structure, instead of the simple collinear AFM. Although films with 4 and 5 ML thickness were not investigated, the possibility of more complex spin alignments in these cases should certainly be investigated.

4. Summary of conclusions

Electronic structure calculations were performed for embedded clusters representing 3, 4 and 5 ML of fcc Fe on Cu(001) with ideal interface, and for the 4Fe/2(FeCu)/1Cu system representing the interdiffusion of Fe and Cu at the interface of the two metals, for FM and several AFM spin configurations.

Calculated magnetic moments are larger at the surface, where they have similar values (2.81–2.89 μ_B) independently of the number of layers or spin configuration.

In all cases, it was obtained that whenever there is AFM coupling among layers, the spin magnetic moments of the Fe atoms in these layers are considerably reduced, with respect to the same layers in the FM configuration.

For the FM spin configurations, the magnitude of the contact HF is larger at the intermediate layers, with respect to the surface and interface. This is due to the valence contribution to B_c having the same sign as the core contribution. In spite of the larger magnetic moment at the surface layers, the magnitude of the contact HF is considerably reduced, due to different signs of the core and valence contributions.

The dipolar HF has non-negligible values at the surface in all cases, with the direction of the principal component perpendicular to the plane of the ML. The sign of the perpendicular component is always opposite to the sign of B_c, thus reducing the magnitude of the total field in this direction. Inversely, the parallel component has the same sign as B_c, and this enhances the total HF in the parallel direction.

For the interdiffusion model 4Fe/2(FeCu)/1Cu, the only significant changes are seen at the mixed Fe–Cu layers; at the upper layers, results converge rapidly to those for the ideal interface.

EFGs are large at the Fe surface in all cases, with similar values around $\sim 5 \times 10^{17}$ V cm^{-2} and direction perpendicular to the surface.

Acknowledgments

This research was partially supported by the CNPq. The authors acknowledge a grant from FAPERJ. Calculations were performed in part at the Cray J90 of the supercomputing centre of the Universidade Federal do Rio Grande do Sul.

References

[1] Moruzzi V L, Marcus P M, Schwarz K and Mohn P 1986 *Phys. Rev.* B **34** 1784
[2] Wang C S, Klein B M and Krakauer H 1985 *Phys. Rev. Lett.* **54** 1852
[3] Uhl M, Sandratskii L M and Kübler J 1992 *J. Magn. Magn. Mater.* **103** 314
[4] Mryasov O N, Gubanov V A and Liechtenstein A I 1992 *Phys. Rev.* B **45** 12330
[5] Macedo W A A and Keune W 1988 *Phys. Rev. Lett.* **61** 475
[6] Macedo W A A, Keune W and Ellerbrock E D 1991 *J. Magn. Magn. Mater.* **93** 552
[7] Keune W, Schatz A, Ellerbrock R D, Fuest A, Wilmers K and Brand R A 1996 *J. Appl. Phys.* **79** 4265
[8] Halbauer R and Gonser U 1983 *J. Magn. Magn. Mater.* **35** 55
[9] Keune W, Ezawa T, Macedo W A A, Glos U, Schletz K P and Kirschbaum U 1989 *Physica* B **161** 269
[10] Ellerbrock R D, Fuest A, Schatz A, Keune W and Brand R A 1995 *Phys. Rev. Lett.* **74** 3053
[11] Pescia D, Stampanoni M, Bona G L, Vaterlaus A, Willis R F and Meier F 1987 *Phys. Rev. Lett.* **58** 2126
[12] Magnan H, Chandesris D, Villette B, Heckmann O and Lecamte J 1991 *Phys. Rev. Lett.* **67** 859
[13] Thomassen J, May F, Feldmann B, Wuttig M and Ibach H 1992 *Phys. Rev. Lett.* **69** 3831
[14] Wuttig M and Thomassen J 1993 *Surf. Sci.* **282** 237
[15] Li D, Freitag M, Pearson J, Qiu Z Q and Bader S D 1994 *Phys. Rev. Lett.* **72** 3112
[16] Müller S, Bayer P, Reischl C, Heinz K, Feldmann B, Zillgen H and Wuttig M 1995 *Phys. Rev. Lett.* **74** 765
[17] Heinz K, Müller S and Bayer P 1996 *Surf. Sci.* **352–354** 942
[18] Pizzini S, Fontaine A, Giorgetti C, Dartyge E, Bobo J-F, Piecuch M and Baudelet F 1995 *Phys. Rev. Lett.* **74** 1470
[19] Straub M, Vollmer R and Kirschner J 1996 *Phys. Rev. Lett.* **77** 743
[20] Zharnikov M, Dittschar A, Kuch W, Schneider C M and Kirschner J 1996 *Phys. Rev. Lett.* **76** 4620
[21] Fu C L and Freeman A J 1987 *Phys. Rev.* B **35** 925
[22] Li C, Freeman A J and Fu C L 1990 *J. Magn. Magn. Mater.* **83** 51
[23] Fernando G W and Cooper B R 1988 *Phys. Rev.* B **38** 3016
[24] Guenzburger D and Ellis D E 1995 *Phys. Rev.* B **51** 12519
[25] Guenzburger D and Ellis D E 1995 *Phys. Rev.* B **52** 13390
[26] Újfalussy B, Szunyogh L and Weinberger P 1996 *Phys. Rev.* B **54** 9883
Szunyogh L, Újfalussy B and Weinberger P 1997 *Phys. Rev.* B **55** 14392
[27] Asada T and Blügel S 1997 *Phys. Rev. Lett.* **79** 507
[28] Moroni E G, Kresse G and Hafner J 1999 *J. Phys.: Condens. Matter* **11** L35
[29] Moroni E G, Kresse G and Hafner J 1999 *J. Magn. Magn. Mater.* **198/199** 551
[30] Spišák D and Hafner J 2000 *Phys. Rev.* B **61** 16129
[31] Guo G Y and Ebert H 1996 *Phys. Rev.* B **53** 2492
Guo G Y and Ebert H 1996 *Hyperfine Interact.* **97/98** 11
[32] Popescu V, Ebert H, Szunyogh L, Weinberger P and Donath M 2000 *Phys. Rev.* B **61** 15241
[33] Peduto P R and Frota-Pessôa S 1997 *Bras. J. Phys.* **27** 574
[34] Allenspach R 1994 *J. Magn. Magn. Mater.* **129** 160
[35] Kirk K J 2000 *Contemp. Phys.* **41** 61
[36] Heinrich B and Bland J A C (eds) 1994 *Ultrathin Magnetic Structure* vols 1 and 2 (Berlin: Springer)
[37] Ellis D E 1968 *Int. J. Quantum Chem.* **2S** 35
Ellis D E and Painter G S 1970 *Phys. Rev.* B **2** 2887

[38] Ellis D E and Guenzburger D 1999 The discrete variational method in density functional theory and its applications to large molecules and solid-state systems *Adv. Quantum. Chem.* **34** 51
[39] Parr R G and Yang W 1989 *Density Functional Theory of Atoms and Molecules* (New York: Oxford University Press)
[40] Gómez J A and Guenzburger D 2001 *J. Magn. Magn. Mater.* **226–230** 381
[41] Vosko S H, Wilk L and Nusair M 1980 *Can. J. Phys.* **58** 1200
[42] Ceperley D M and Alder B J 1980 *Phys. Rev. Lett.* **45** 566
Ceperley D M 1978 *Phys. Rev.* B **18** 3126
[43] Delley B and Ellis D E 1982 *J. Chem. Phys.* **76** 1949
[44] Mulliken R S 1955 *J. Chem. Phys.* **23** 1833
Mulliken R S 1955 *J. Chem. Phys.* **23** 1841
[45] Abragam A 1961 *The Principles of Nuclear Magnetism* (Oxford: Oxford University Press)
[46] Gómez J A and Guenzburger D 2001 *Phys. Rev.* B **63** 134404
[47] Greenwood N N and Gibb T C 1971 *Mössbauer Spectroscopy* (London: Chapman and Hall)
[48] Lindgren B 1990 *Europhys. Lett.* **11** 555
[49] Blaha P, Schwarz K and Dederichs P H 1988 *Phys. Rev.* B **37** 2792
[50] Schmitz D, Charton C, Scholl A, Carbone C and Eberhardt W 1999 *Phys. Rev.* B **59** 4327
[51] Dunn J H, Arvanitis D and Mårtensson N 1996 *Phys. Rev.* B **54** R11 157
[52] Qian D, Jin X F, Barthel J, Klaua M and Kirschner J 2001 *Phys. Rev. Lett.* **87** 227204–1